Thermal Induced Phase Transformations in Mg-PSZ Fine-grain Ceramics Investigated by XRD and EBSD

H. Berek, C.G. Aneziris, C. Wenzel, T. Westphal, W. Schärfl

Phase transformation in partly stabilized zirconia (PSZ) is of great importance especially in connection with transformation toughening effects in composites. For the phase analysis X-ray diffraction (XRD) and transmission electron microscopy (TEM) are well established methods. Electron backscatter diffraction (EBSD) yields interesting additional information regarding the combination of high spatial resolution and integral phase analysis. Unfortunately, the results of XRD and EBSD investigations may differ. This paper describes the influence of the sintering temperature and an additional heat treatment on the phase composition of Mg-PSZ as determined by XRD and EBSD.

1 Introduction

Zirconia appears in three modifications. The monoclinic phase (m-ZrO_2) is thermodynamically stable and exists below 1170 °C. Above this temperature the tetragonal modification (t-ZrO_2) occurs. At temperatures higher than 2370 °C up to melting the cubic phase (c-ZrO_2) is stable. The t→m transformation has a great importance for the mechanical properties of zirconia components.

Harry Berek, Christos G. Aneziris, Claudia Wenzel, Torsten Westphal, Wolfgang Schärfl
Technical University Mining Academy Freiberg
Institute of Ceramic, Glass and Construction Materials
09599 Freiberg, Germany

Corresponding author: *H. Berek*
E-mail: harry.berek@ikgb.tu-freiberg.de

Keywords: Mg-PSZ, EBSD phase analysis, XRD, phase transformation

Received: 20.10.2010
Accepted: 19.01.2011

It appears with a volume change of 3 – 5 % and exceeds the critical fracture length in ceramics. Additions of Y_2O_3, CaO or MgO are used to stabilise t- and c-phases to room temperature (Fig. 1). The high strength and fracture toughness of partially stabilised zirconia is based on the phase transformation t→m during crack growth. Thus during crack growth a processing zone that is under compressive strain is developed around the crack tip [1]. In this way further crack growth is reduced. It is considered in the literature that thermal induced phase transformation in cubic zirconia starts with the formation of tetragonal lenses in the range of 250 nm on special lattice planes [2, 3, 4]. This could be shown by TEM investigations. The destabilisation of PSZ is connected with Mg grain boundary diffusion [5] and can result in the formation of $Mg_2Zr_5O_{12}$ [3]. Thus the development of new phase analysis strategies is important with the goal of a full understanding of these transformation processes.
XRD measurements yield information about the integral composition. There are limits concerning the minimum grain size and partition of a certain modification within the sample. The EBSD method has advantages especially regarding the spatial resolution. But it is difficult to measure global concentrations. Differences in the excited sample regions are to be taken into account. Therefore a comparison of the results of these different methods became necessary. This paper describes the influence of the sintering temperature and an additional thermal treatment on the phase composition of PSZ as determined by XRD and EBSD.

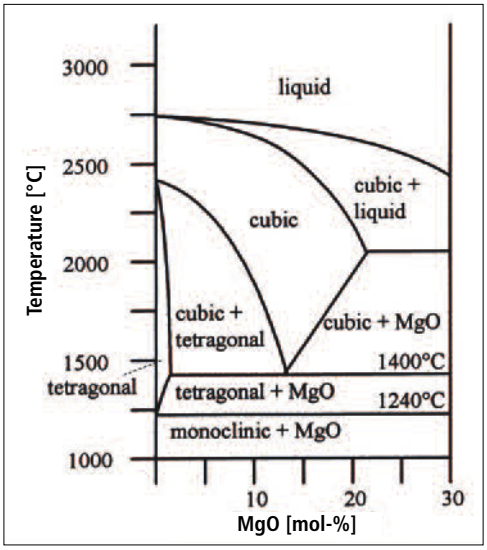

Fig. 1 Phase diagram of partly MgO-stabilized ZrO_2 [15]

2 Experimental

Composite specimens were prepared from 3,4 mass-% magnesia partially stabilised zirconia (Mg-PSZ, *Saint Gobain*/USA). The Mg-PSZ powder had a mean particle size of 1,3 µm. Its chemical composition is listed in Tab. 1.
The starting powders were mixed with deionised water with a weight ratio powder : water of 70 : 30. A synthetic polyelectrolyte (KM 1001) and a hydrocolloid (KM 2000) provided by *Zschimmer & Schwarz* / DE, were used to disperse and stabilise the suspension. To improve the strength of the green bars Optapix PAF 35 (Zschimmer & Schwarz) was used. The raw materials were mixed for 2 h in a polypropylene chamber

Tab. 1 Chemical composition of the Mg-PSZ powder [mass-%]

ZrO_2	MgO	Al_2O_3	SiO_2	HfO_2	CaO	TiO_2	Na_2O	Fe_2O_3
91,39	3,37	0,63	2,43	1,73	0,21	0,14	0,09	0,01

Tab. 2 Lattice parameters used in the EBSD and XRD phase analysis

Phase	Remarks	Crystal system	Lattice parameters					
			a [Å]	b [Å]	c [Å]	α [deg]	β [deg]	γ [deg]
ZrO_2	EBSD	monoclinic	5,1507	5,2038	5,3156	90	99,196	90
ZrO_2	XRD	monoclinic	5,145	5,207	5,311	90	99,2	90
ZrO_2	EBSD	tetragonal	3,5794	3,5794	5,1647	90	90	90
ZrO_2	XRD	tetragonal	3,596	3,596	5,184	90	90	90
ZrO_2	EBSD	cubic	5,09	5,09	5,09	90	90	90
ZrO_2	XRD	cubic	5,086	5,086	5,086	90	90	90

with zirconia milling media. Using slip casting technology, rectangular bars with 3,5 x 4,5 x 40 mm^3 have been manufactured.

The de-binding step took place at 400 °C in an oxidising atmosphere with a heating rate of 1 K/min and a holding time of 2 h. Afterwards the bars were sintered in an electrical furnace in oxidising atmosphere. The heating rate was 3 K/min to 1450 °C, 1550 °C and 1650 °C, respectively. The holding time at sintering temperature was 3 h, and the cooling rate 5 K/min to room temperature. After sintering the shrinkage was measured. Open porosity and bulk density were determined with the aid of mercury porosimetry (PASCAL series, *Porotec*/DE). For the materials sintered at 1450 °C the open porosity was 21,79 %, at 1550 °C it was determined with 14,84 % and by sintering at 1650 °C an open porosity of 10,88 % was measured. The thermal expansion of the Mg-PSZ ceramics was determined using a dual rod dilatometer (DIL 402 from *Netzsch*/DE). The samples were cycled three times between room temperature and 1300 °C. During the thermal hysteresis the heating and cooling rate was 4 K/min. The resulting data (per cent elongation plotted against temperature) were used to examine changes in the transformation characteristics arising from the high-temperature exposure. After the second thermal hysteresis the phase composition was investigated by EBSD and XRD.

XRD measurements have been performed on a PANalytical X'Pert Pro MPD with a PIXcel detector in Bragg-Brentano geometry. The bar-shaped samples from EBSD analysis were cleaned and mounted on a special sample holder without further preparation. The polished face was analysed. The measurements were done with rotating samples. Following measurement conditions were always applied: Cu tube with 40 kV / 40 mA, angular range $20° < 2\theta < 110°$, effective step size 0,013°, and effective counting time 29 s per step. The Rietveld method was used for quantitative phase analysis.

Topas- and HighscorePlus-software was used to perform the Rietveld analyses. Same structure models have been used for each sample as base for quantitative phase analyses. The structure models were taken from a special version of ICSD [6]. Unfortunately, it was not possible to separate the phases and to analyse them individually. Therefore the structure models could not be fully adapted to the actual material. Lattice and peak shape parameters have been refined but atomic coordinates, site occupancies, and temperature factors were left fixed. R_{WP}-values from 8 to 10 were obtained for each sample.

The Rietveld method is a calculation procedure to analyse powder diffraction patterns. It has been originally developed by *H.M. Rietveld* [7, 8] for crystal structure determination using neutron diffraction. It has been

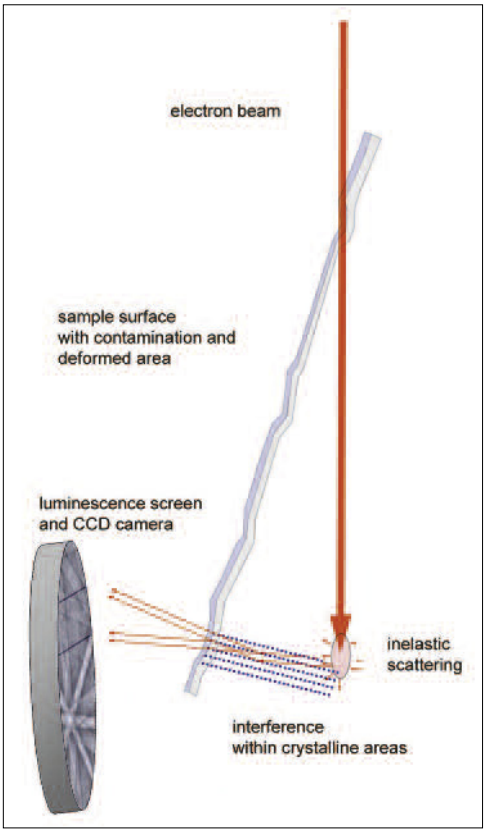

Fig. 2 Principle of electron backscatter diffraction (EBSD)

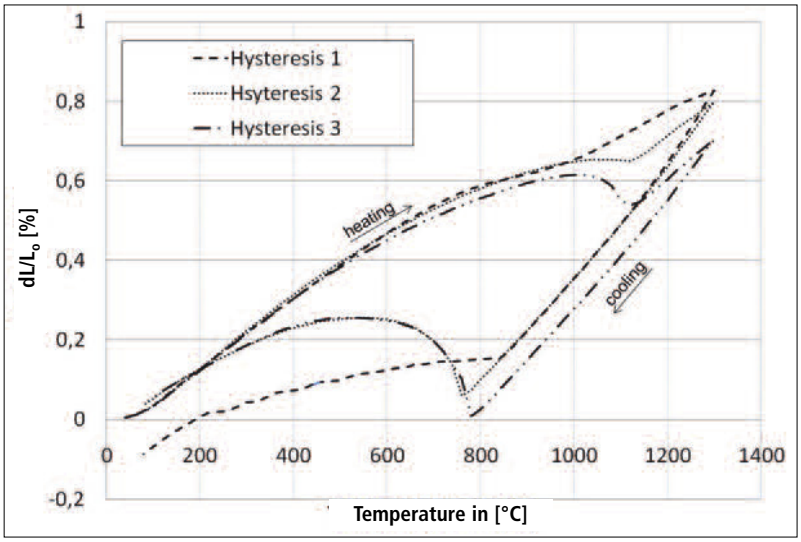

Fig. 3 Thermal expansion curves of the Mg-PSZ ceramic sintered at 1450 °C

later adapted to X-ray diffraction. Since the last decade of the 20th century the Rietveld method became a wide-spread tool for quantitative phase analysis.

With powder diffraction an integrated signal over a radiated area is measured. The radiated area consists of a large number of grains containing individual crystalline structures. Therefore, the powder diffraction pattern of a sample is a superposition of a large number of individual patterns. With the Rietveld method the diffraction pattern of the sample is unfolded into patterns of single phases. The scale of each single phase pattern is taken as a measure of the amount of this phase. Generally the profile refinement strategy included a lattice parameter refinement within the limits ±0,005 nm and ±1,0° respectively. The coherent diffracting area size was in the range between 50 nm and 500 nm. Strain or preferred orientation was not considered.

Microstructure characterisation was conducted using scanning electron microscopy (SEM), energy dispersive X-ray microanalysis (EDX) as well as electron backscatter diffraction (EBSD). Overviews regarding the EBSD method are given in several contributions [9, 10]. Electron backscatter patterns (EBSP) contain all information about the lattice symmetry within the excited sample volume (about 20 to 100 nm) and thus can be used for phase analysis. They consist of parallel lines for each reflecting lattice plane. The angles between these lines in the so called Kikuchi pattern or EBSP exactly correspond to the angle in the lattice structure. The analysis is realised by comparing the measured angles with calculated ones. There is a possibility to determine lattice spacing too. But under normal conditions for ceramic materials the accuracy is not acceptable. The basic principle is given in Fig. 2. The incident electron beam is scattered un-elastically within the sample. A part of the backscattered electrons can escape the sample. In their way they are reflected on lattice planes. The EBSP is a result of interference following Braggs rule. In the case of ceramic materials a conductive coating is necessary. One also should keep in mind that as a result of sample preparation a disturbed region might occur. These effects strongly reduce the quality of EBSP.

Phase determination can be carried out for single spots or for defined scans. There are

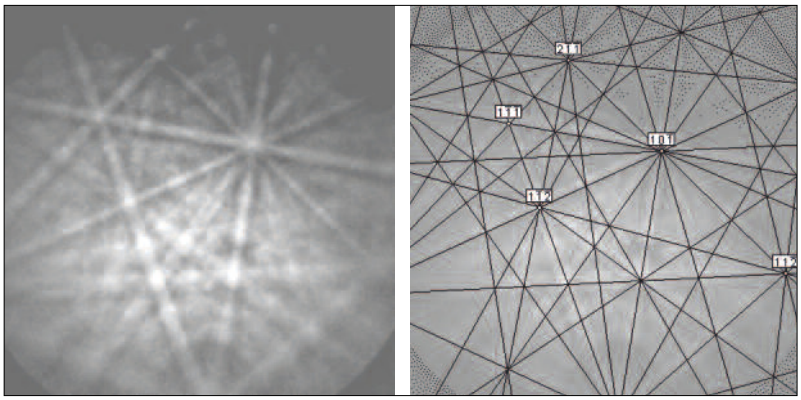

Fig. 4 Typical EBSP of cubic ZrO_2 and corresponding indexing

two preconditions for a successful EBSD phase mapping. First of all undisturbed and electrically conducting sample surfaces are needed. Sample preparation thus is of great importance especially in the case of multi crystalline ceramic materials which contain a high number of cracks. The second problem to be solved is a set of lattice parameters of phases which really are involved in the given sample. We used an ICDD data base [11]. By comparison of the EBSD results with X-ray diffraction a set of possible crystal structures was defined. The results for the given PSZ materials are given in Tab. 2.

The sample preparation was realised by vibration polishing in a Buehler VibroMet2. All samples were coated with some nanometre thick Pt-layers using a conventional Edwards sputter coater. EBSD investigations were performed in a Philips XL30 microscope equipped with an EDAX TSL EBSD system.

3 Results

The thermal expansion curves of the Mg-PSZ ceramic sintered at 1450 °C, 1550 °C and 1650 °C respectively show a lowering of expansion after each cycle from room temperature to 1300 °C. Fig. 3 shows one example. Due from tetragonal to monoclinic transformation the thermal expansion has a non-linear behaviour. A typical hysteresis is observed. The reduction of thermal expansion after each cycle can be explained by micro-cracking due to the repeated phase transforma-

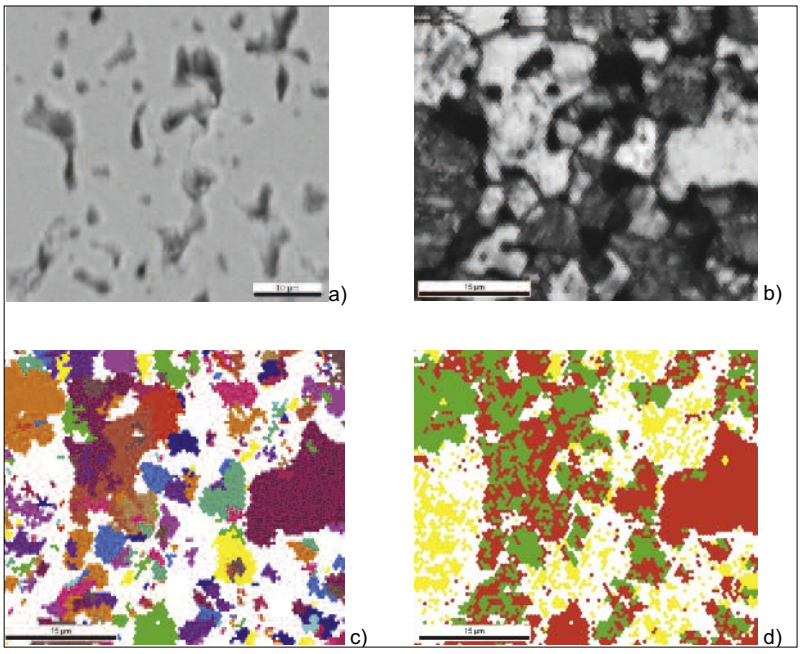

Fig. 5 Sample PSZ, sintering temperature 1550 °C and an additional thermal cycling between room temperature and 1300 °C (dilatometer)
a) SE image; b) EBSD quality map; c) EBSD misorientation map; d) EBSD phase map, showing cubic ZrO_2 (green), tetragonal ZrO_2 (red) and monoclinic ZrO_2 (yellow)

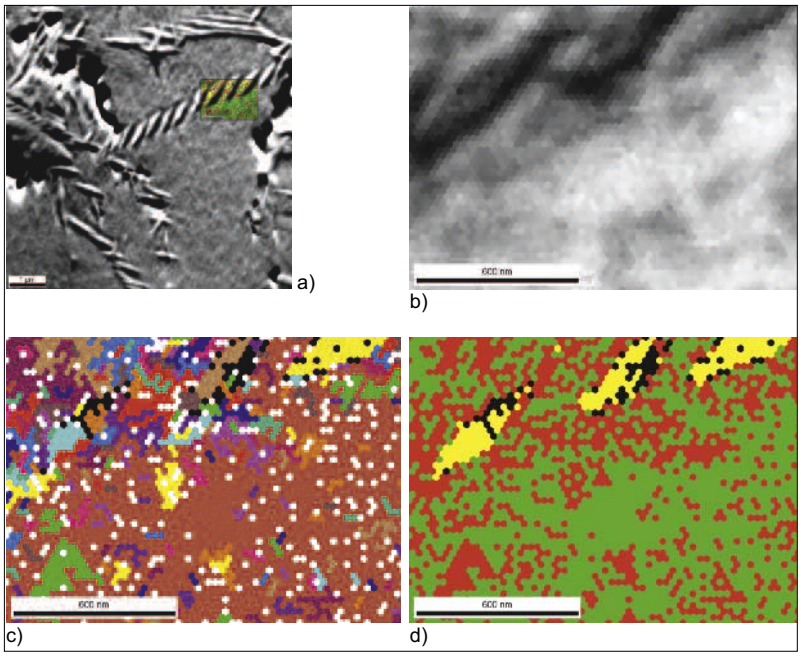

Fig. 6 Sample PSZ, sintering temperature 1650 °C; SE image and EBSD analysis of an area with monoclinic lenses
a) typical SE image with scanned area; b) EBSD quality map; c) EBSD misorientation map; d) EBSD phase map showing cubic ZrO_2 (green), tetragonal ZrO_2 (red) and monoclinic ZrO_2 (yellow) (Courtesy Dr Rene de Kloe, EDAX)

tion in connection with enhanced destabilisation [12]. During cooling, the tetragonal to monoclinic transformation leads to an expansion below 790 °C. In the first hysteresis a negative thermal expansion of 0,1 % occurs. This can be explained with a remaining sintering shrinkage during the first hysteresis from room temperature to 1300 °C.

A typical EBSP is given in Fig. 4. Each diffraction pattern leads to a decision for one of the involved phases (see Tab. 2). In the given case this is cubic ZrO_2. As parameters the number of identified lattice planes corresponding to Kikuchi bands and the median angle difference between model and experiment for the angles between those lattice planes were used. For each sample 10 arbitrary distributed scan areas were investigated. One example is shown in Fig. 5. The scan area was about 50 µm x 50 µm. In the SE image (a) one can realize a rather smooth surface after polishing with some porosity. Note that ZrO_2 is not conducting and thus needs to be coated electrically for SEM investigations. The layer thickness is the result of an optimization process. On the one hand the layers have to be thick enough in order to avoid charging effects. On the other hand they have to be thin enough in order not to disturb the diffraction patterns. Therefore there is always some noise in the SE images. The pores clearly are recognizable in the EBSP quality map showing black contrast. Patterns in these areas of poor EBSP quality cannot be identified. The same holds for grain boundaries where lattice defects and overlapping also lead to undefined patterns. The orientation map (c) is used to identify different grains by their orientation differences. In the given case the phase map (d) shows cubic, tetragonal and monoclinic ZrO_2 respectively. Phase transformations always start at crystallization sites inside of the cubic grains as was already shown in [2] and [13] by TEM investigations. Transition phases are to be taken into account. But the dominating route goes from cubic over tetragonal to the stable monoclinic phase in PSZ. In SEM investigation one finds oriented monoclinic lenses within cubic grains as a result of destabilisation as could be shown in [4]. One example for this kind of monoclinic precipitations is given in Fig. 6. Note that monoclinic lenses are found within cubic grains containing a high number of small tetragonal phases. They are distributed inhomogeneously within the samples. Thus tetragonal phases seem to act only as crystallisation sites and are disappearing after some growth of the monoclinic lenses. Corresponding results of the phase analysis in comparison with XRD measurements are given in Tab. 3.

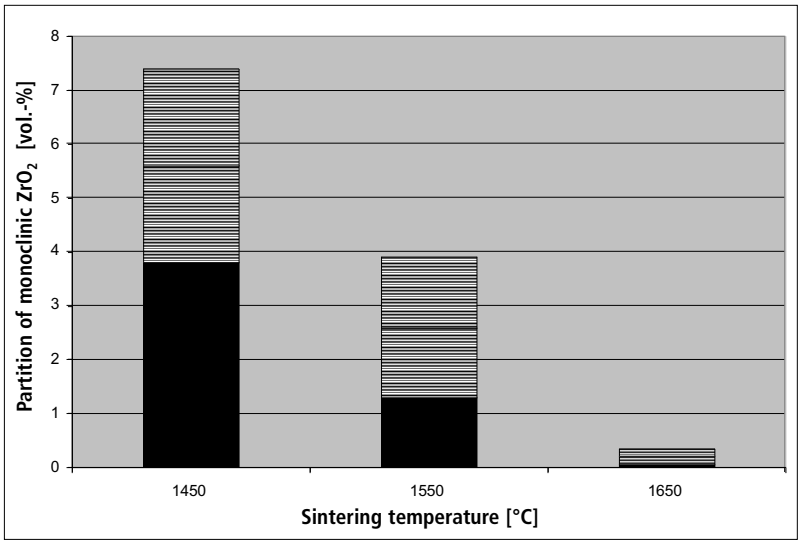

Fig. 7 Partition of monoclinic ZrO_2 as determined by EBSD in dependence on the sintering temperature, and corresponding standard deviations

Fig. 7 shows the influence of the sintering temperature on the phase composition of PSZ. Hence sintering was carried out in the stability region of cubic and tetragonal ZrO_2 respectively. Higher temperature leads to a smaller partition of monoclinic phases comparing to the powder. On the other hand an additional heat treatment results in a recrystallization of monoclinic ZrO_2 as is shown in Fig. 8. At the same time tetragonal ZrO_2 is destabilized due to Mg-diffusion. Mg was found in spinel precipitations on grain

boundaries by using combined EBSD/EDX investigations.

A typical XRD pattern of PSZ is shown in Fig. 9. In the given range of 2 θ values the problem of overlapping of cubic and tetragonal peaks can be recognized. Monoclinic peaks are separated clearly. The resulting lattice parameters in the Rietveld analysis are listed in Tab. 2. It was concluded that as a result of XRD analysis only the sum of the cubic and tetragonal partition is given (see Tab. 3).

4 Discussion and conclusions

The thermal expansion curves show a broad transition range between 700 °C and 1200 °C. This range corresponds to the phase transformation between the tetragonal and monoclinic phases. The observed increase of the hysteresis after each thermal cycle can be explained by a growing defect density especially micro cracking. On the other hand due to the Mg diffusion in dependence on temperature and time a rising destabilisation of the cubic and tetragonal phases takes place. The state of the material more and more compares to the not stabilized zirconia with some Mg containing precipitations on grain boundaries.

The comparison of XRD- and EBSD-phase analyses shows principal differences. First of all the different excited sample volumes are to be considered. The median particle size of the zirconia powders used was 1,3 µm; thus the size of crystallites is much smaller. As EBSD investigations at higher magnification clearly showed phase transitions in PSZ always start within former cubic grains. Growing monoclinic crystals have rather small defect densities in comparison to the remaining cubic and tetragonal areas. The observed tetragonal lenses seem to act as crystallisation sites for monoclinic crystallites. That's why the transition areas within former cubic grains do not contribute to the XRD phase information. But they are considered in the frame of EBSD measurements. Monoclinic crystals are determined correctly with XRD and EBSD methods. Thus it can be explained why XRD measurements result in higher values of the monoclinic phase content in comparison to EBSD.

EBSD investigations allow phase analysis in PSZ at high spatial resolution. This is an extension to the phase analysis by TEM methods using rather small samples. It becomes clear that inhomogeneities play a more important role than assumed before. The observed typical tetragonal phase in the transition of PSZ is in agreement with [14]. Starting point of the destabilisation of PSZ are tetragonal lenses in the range of 250 nm [2, 3]. It is considered in the literature [3] that destabilization is connected with the formation of $Mg_2Zr_5O_{12}$. This phase never could be found in the frame of the present investigations.

Tab. 3 Partitions of the ZrO_2 modifications as determined by XRD and EBSD in dependence on the sintering temperature

Partition	Remarks	Sintering at 1450 °C	Sintering at 1550 °C	Sintering at 1650 °C
Cubic/tetragonal	XRD	72	87	97
Monoclinic	XRD	28	13	3
Cubic	EBSD	30,0 ± 4,3	30,2 ± 5,7	89,9 ± 3,7
Tetragonal	EBSD	64,4 ± 3,7	67,2 ± 5,6	9,8 ± 3,4
Monoclinic	EBSD	5,6 ± 1,8	2,6 ± 1,3	0,2 ± 0,1

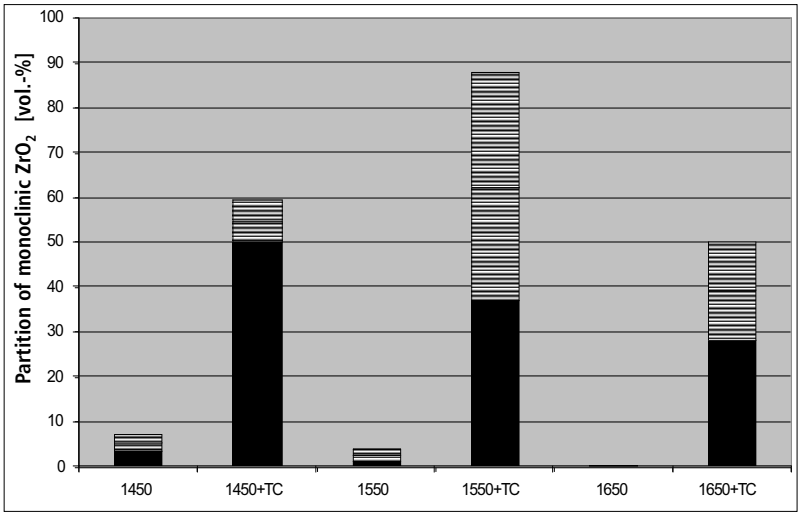

Fig. 8 Partition of monoclinic ZrO_2 as determined by EBSD in dependence on the sintering temperature (6 h) and an additional thermal cycling between room temperature and 1300 °C (dilatometer)

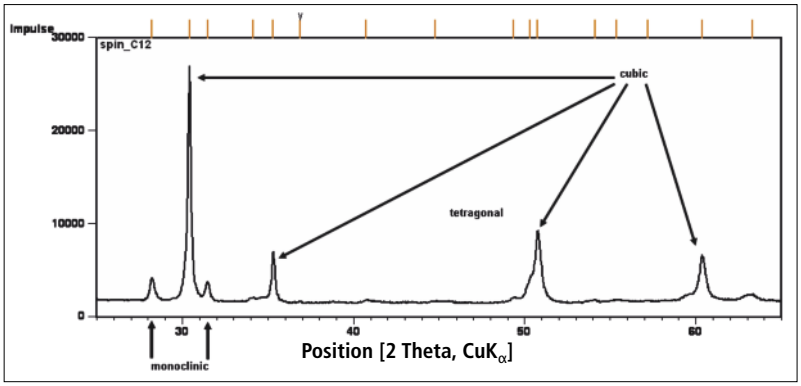

Fig. 9 Typical XRD spectrum of PSZ in the small angle range with overlapping of the cubic and tetragonal peaks

References

[1] Lin, K.L.; Lin, C.C.: Reactions between titanium and zirconia powders during sintering at 1550 °C. J. Am. Ceram. Soc. 98 (2007) 2220–2225

[2] Hannink, R.H.J.: Microstructural development of sub-eutectoid aged MgO-ZrO_2 alloys. J. Mat. Sci. 18 (1983) 457–470

[3] Hannink, R.H.J.; Kelly, P.M.; Muddle, B.C.: Transformation toughening in zirconia-containing

ceramics. J. Am. Ceram. Soc. 83 (2000) 461–487

[4] Aneziris, C.G.; Pfaff, E.M.; Maier, H. R.: Fine grained Mg-PSZ ceramics with titania and alumina or spinel additions for near net shape steel processing. J. Eur. Ceram. Soc. 20 (2000) 1729

[5] Sakka, Y.; Oishi, Y.; Ando, K.: Enhancement of MgO evaporation from MgO-stabilized ZrO_2 by grain-boundary diffusion. J. Am. Ceram. Soc. 69 (1986) 111–113

[6] PAN-ICSD Version 1.3: International centre of structure data (ICSD), PANalytical b.v., 2007

[7] Rietveld, H.M.: Line profiles of neutron powder-diffraction peaks for structure refinement. Acta Crystallogr. 22 (1967) 151–152

[8] Rietveld, H.M.: A profile refinement method for nuclear and magnetic structures. J. Appl. Cryst. 2 (1969) 65–71

[9] Schwartz, A.J.; Kumar, M.; Adams, B.L.: Electron backscatter diffraction in materials science. Kluwer Academic/Plenum, New York, 2000

[10] Humphreys, F.J.: Review: grain and subgrain characterisation by electron backscatter diffraction. J. Mat. Sci. (2001)

[11] ICDD PDF-2 database release 2008, International Centre for Diffraction Data (ICDD), 2008

[12] Becher, P.F.; Ferber, M.K.: Mechanical behaviour of MgO-partially stabilized ZrO_2 ceramics at elevated temperatures. J. Mat. Sci. 22 (1987) 973–980

[13] Chaim, R.; Brandon, D.G.: Microstructure evolution and ordering in commercial Mg-PSZ. J. Mat. Sci.19 (1984) 2934–2942

[14] Hill, R.J.; Reichert, B.E.: Measurement of phase abundance in magnesia partially stabilized zirconia by Rietveld analysis of X-ray diffraction data. J. Am. Ceram. Soc. 73 (1990) 2822–2827

[15] Stevens, R.: An introduction to zirconia, No 113: Magnesia electron publication. Shervin Rivers Ltd, 1983